Impact of open-air processing on atmospheric pressure plasma deposition of poly(ethylene oxide) coatings for antifouling applications

Tijs Dekoster[a,b]; Rita Vos[b]; Karolien Jans[b]; Willem Van Roy[b]; Bernard Nisol[c]; Bastien Duckert[a,b]; Anja Vanleenhove[b], Annelies Delabie[b,a]

a) KU Leuven, Kwantumchemie en Fysicochemie Celestijnenlaan 200f, B3001 Leuven
b) Imec, Kapeldreef 75, B3001 Leuven, Belgium
c) Molecular Plasma Group, Gaston Geenslaan 1, B3001 Leuven

Abstract

Atmospheric Pressure Plasma Deposition (APPD) of poly(ethylene oxide) (PEO)-like antifouling coatings provides an attractive way to reduce biofouling for reliable biosensor operation. Cold atmospheric pressure plasma jets are designed to operate in open air. This paper demonstrates the impact of open-air processing on the composition and properties of PEO-like coatings by APPD with vinylether precursors. The open-air environment inhibits polymerization as indicated by low deposition rates, oxygen incorporation in the coatings and instability of the coatings in water. The composition and stability of the coatings improve by appropriate nozzle design and by deposition in an environment with lower air content. The resulting PEO-like coatings are stable and antifouling for an antibody solution and inhibit adhesion of human fibroblast cells.

Keywords: Antifouling, atmospheric pressure plasma, poly(ethylene glycol), inhibition of polymerization, poly(ethylene oxide), chemical vapor deposition, plasma-enhanced chemical vapor deposition, open-air processing, organic thin films, polymer coatings

Introduction

The past few years, the interest in biosensors has surged [1]. Their performance and lifetime are often limited by the undesired binding of proteins and cells to the device surface, something referred to as biofouling. For example in immunoassays, non-specific binding of analyte leads to false-positive results [2]. In electrochemical sensors, fouling can lead to decreased sensitivity and device lifetime due to the formation of an impermeable layer for the analyte [3]. For implants or catheters biocompatibility is important to prevent inflammation and encapsulation of the device [4]. This underlines the need for suitable interface chemistries to match the inorganic device surface with a biological environment. A good strategy to address this is to implement poly(ethylene oxide)- layers (PEO-layers), also known as poly(ethylene glycol) layers, that are considered as the "gold standard" for antifouling layers [5]. Several approaches for surface modification with PEO exist, including the use of PEO-based self-assembled monolayers (SAMs) [6–8], grafted PEO polymer brushes [9–12], and the deposition of PEO coatings by photopolymerization [13,14] and plasma deposition (PD).

PD provides a solvent free way to deposit PEO layers. The early research on PEO PD focused on low-pressure plasmas, which requires expensive vacuum chambers [15–19]. In recent years, atmospheric pressure plasma deposition (APPD) is receiving increased attention thanks to the low cost of the APPD equipment and its potential for scaling up the production [20–27]. Typical precursors for PEO APPD are tri(ethylene glycol) dimethyl ether and tetra(ethylene glycol) dimethyl ether [15,17,23,25]. To obtain stable antifouling layers by APPD, we need to preserve the functional groups, the ethylene oxide (also called ethylene glycol, EG) units, during the APPD process while enabling cross-linking to obtain a stable coating. In this work, we use a dielectric barrier discharge cold atmospheric pressure plasma jet (CAPjet) and we inject the precursor in the post-discharge region. Precursor injection in the post-discharge region can enable soft polymerization initiated by metastable species and radicals with retention of the functional groups [29]. In this approach, the precursors should include the functional groups as well as more reactive chain ends that will more readily react in plasma to promote precursor cross-linking. The plasma can in principle break any bond in the precursor, but unsaturated bonds such as C-C double bonds are preferentially activated, preserving other parts of the precursor [30,31]. Therefore, PEO-precursors with vinyl end groups are promising precursors for PEO APPD with CAPjet.

This paper investigates the impact of the open-air environment on the APPD of PEO layers, using an open-air CAPjet in an indirect configuration with precursor injection in the post-discharge region. We use di(ethylene glycol) divinyl ether (2EGDVE) as precursor (Figure 1) because it contains two ethylene glycol units and it has two vinyl functions for preferential activation to enable cross-linking [30]. CAPjets are

designed to operate in open air with inert gas flows that should limit the impact of air on the deposition. Still, if residual air unintentionally reaches the plasma region it could change the plasma composition and deposition process by inhibiting the polymerization reaction [30,32,33]. In addition, reactive oxygen and nitrogen species (ROS and RNS) can be generated [34,35]. However, the role of air during PEO APPD with an open-air CAPjet is currently not well understood. Therefore, we investigate the effect of the open-air processing on the coating composition and stability in water by reducing the air content in the environment and by using different nozzle shapes. The composition of the obtained coatings is analyzed with Fourier-Transform Infrared spectroscopy (FT-IR), X-ray photoelectron spectroscopy (XPS) and ellipsometry. The impact of the nozzle shape is also investigated theoretically by a computational fluid dynamics (CFD) simulation. Finally, the antifouling properties of the coatings are investigated by measuring the binding of a fluorescently labeled antibody solution and by testing the adhesion of human fibroblast cells.

Materials and methods

Chemicals

2EGDVE (Figure 1), acetic acid, toluene and anti-mouse IgG antibody labelled with an Atto647N fluorescent dye were purchased from Sigma Aldrich, 3-[methoxy(polyethyleneoxy)6-9]propyltrimethoxysilane was purchased from Gelest and 11-azidoundecyltrimethoxysilane was purchased from abcr GmbH. Acetone and isopropanol were purchased from CMC materials.

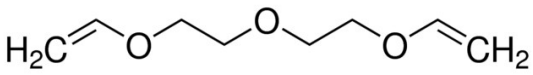

Figure 1: Di(ethylene glycol) divinyl ether (2EGDVE) precursor structure

Substrates

P-type silicon wafers with ⟨100⟩ crystal orientation (purchased from MEMC Electronic Materials) were precleaned using a two-step cleaning sequence with an O_3 based step for oxidation and diluted HF for subsequent oxide removal [36]. A clean chemical oxide was regrown using ozonated deionized water (DIW) in the final rinsing step. The thickness of the oxide is around 1 nm, as was verified using ellipsometry and is not affected by subsequent air exposure. The wafers were then cleaved into 3 cm x 3 cm coupons. Particles generated during cleaving were removed by subsequent sonication in acetone and isopropanol

for 10 minutes. Immediately before plasma deposition, the substrates received an additional 15 min UV/O_3 clean (UVO-cleaner, Jelight Company Inc.) to remove any airborne organic contamination. The oxide thickness of 1 nm was not affected by this treatment. Silicon coupons with a 100nm thermal oxide were used for antifouling measurements and cell adhesion testing.

Plasma deposition

All plasma depositions were performed using the PlasmaSpot® (Molecular Plasma Group (MPG), Luxembourg) DBD plasma jet [37]. This R&D system enables the generation of atmospheric pressure cold (near ambient temperature) plasmas. It consists of two concentric tubular electrodes (Figure 2a); the external one is covered with a dielectric layer and is connected to the power source, while the inner one is grounded. The PlasmaSpot® powered electrode was fed with a high-voltage up to 15 kV peak-to-peak, at a frequency in the 40-50 kHz range. The nominal power output was 90 W for all experiments. A fixed flow rate of 80 standard liters per minute (slm) Argon (Alphagaz, Airliquide) was fed to the system acting as discharge gas. Plasma deposition was performed across the entire sample surface area by scanning the plasmajet with a 16 mm/s line speed and a pitch of 2 mm in a serpentine pattern (Figure 2d). The homogeneous coverage of the substrate is ensured by the small serpentine pitch of 2 mm, which is smaller than the width of the used nozzles (2.5 cm and 2.3 cm for the ring and line nozzle respectively). Therefore, during one serpentine scan every part of the substrate is treated multiple times, leading to homogeneous coverage.

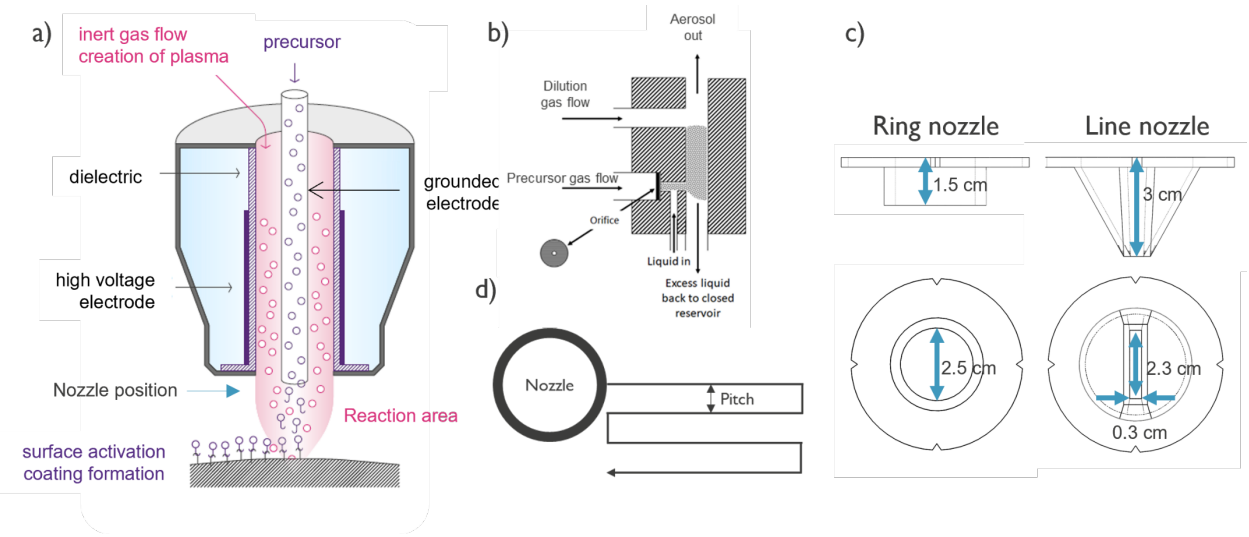

Figure 2: a) Schematic of the plasma deposition tool used for the experiments. b) Schematic of the MPG atomizer used for aerosol generation c) Drawing of the 3D-printed nozzles used to shield the reaction area from air d) Sketch of the scanning motion of the plasma jet.

To shield the reaction area from air, a 3D-printed nozzle was attached to the PlasmaSpot®. In this nozzle the plasma is combined with the precursor. Two nozzle designs were investigated, a line-shaped one and a ring-shaped one (Figure 2c). Due to the different length of the nozzles (1.5 cm and 3 cm for ring and line respectively), the distance between the substrate and the plasma region is longer for the line nozzle. The line nozzle is also narrower than the ring nozzle. The nozzle to substrate distance was fixed to 2 mm. For depositions in an environment with low air content, a flexible plastic foil was attached to the plasma torch and to the substrate holder. During deposition, this plastic foil was inflated by the argon gas flow, resulting in an argon flux which removes air from the deposition area. Small openings were left such that argon gas could escape. The O_2 level inside was checked with a Drager Pack 6000 oxygen sensor and was below 0.2%. Before deposition, the environment was purged for 30 seconds with 80 slm argon to remove the air.

The 2EGDVE precursor has a low vapor pressure which makes it difficult to supply in the vapor phase at atmospheric pressure, but injection of the precursor in the APPD reactor as an aerosol provides an attractive solution. The aerosol was generated by an MPG atomizer. The working principle of the atomizer is described in detail elsewhere [37]. In brief, a primary gas flow (precursor gas flow) accelerates through a circular orifice, which draws up liquid from the precursor bottle through Venturi effect. The liquid is atomized by the high gas velocity, and a secondary gas flow, the dilution flow, is used to dilute the aerosol and transport it to the plasma. An argon flow of 0.8 slm was used as primary flow for atomization of 2EGDVE. This results in a 2EGDVE mass flow of ~7.5 mg/min. The dilution flow was fixed at 5 slm. The orifice size was 0.4 mm.

CFD simulation

A computational fluid dynamics (CFD) simulation was performed using Ansys Fluent 2022 R1. The simulation domain consisted of the plasma torch, nozzle and an air volume surrounding the nozzle, see Supplementary figure 1 for the detailed geometry. The mesh was generated using the Ansys Workbench meshing tool. The coordinate system was cartesian and the mesh contained a total 438 596 and 502 667 elements for the ring and line nozzle simulation, respectively. The argon and air gas species during deposition were considered, while the precursor itself, the plasma excitation and their influence on the flows was not taken into account. Species transport was activated and turbulence was modeled with a standard K-epsilon 2 equation model with standard wall functions. The properties of the species were imported from the Fluent material database. For a normal air environment, the molecular weight was 28.96 g/mol, the density 1.23 kg/m^3 and the viscosity 1.75 10^{-5} kg/m/s. The simulation contained two

velocity inlets and one pressure outlet. Argon gas flows of 46 and 2.5 m/s, corresponding to a gas flow of 80 and 5.7 slm respectively, were considered through the plasma gas and precursor carrier gas velocity inlets (figure 2a). Air was allowed to enter the simulation only via the pressure outlet through backflow. The gauge pressure at this outlet was set at 0 Pa. For argon, the molecular weight was 39.9 g/mol, density of 1.62 kg/m^3 and viscosity of 2.13 x 10^{-5} kg/m/s. The inlet gas temperature was 300 K. A pressure-based solver was used for computation, and the conservation of mass, momentum and energy was activated. Pressure and velocity were coupled and the discretization was, respectively, second order for pressure, second order upwind for momentum, first order upwind for turbulent kinetic energy and turbulent dissipation rate, and second order upwind for the species. Hybrid initialization was performed before the iteration process. The convergence criteria for the residuals were set to: 10^{-4} for the continuity equation, 10^{-6} for energy equation and 10^{-3} for the velocity equations.

Film characterization

The bulk chemical composition of the deposited films was studied by FT-IR in transmission mode using a Nicolet 6700 system from Thermofisher. 60 scans per sample were performed from 400 cm^{-1} to 4000 cm^{-1} with a resolution of 4 cm^{-1}. The background was corrected by subtracting the spectrum of a blank silicon coupon, obtained right before the measurements. TQ-analyst (Thermofisher) software was used to obtain the integrated area of the vibration bands, enabling quantitative analysis.

The composition of the deposited films was further analyzed by XPS measurements using a QUANTES instrument from Physical electronics. The measurements were performed using a monochromatized photon beam (Al Kα: hv = 1486.6 eV), the pass energy was 69 eV and the step size 0.125 eV. Charge compensation was used. Note that the exact quantification of the components of the C 1s peak is dependent on the chosen fitting parameters. The background was corrected using a Shirley model.

The thickness of the deposited films was determined using an RC2 ellipsometer from J. A. Woollam. The samples were measured at an angle of 50, 60, 70 and 80 degrees for 3 seconds at every angle. The data was fitted using the CompleteEASE software with a two-layer model on a silicon substrate, consisting of a native silicon oxide layer described by a Ntve_JAW3 model and the polymer film fitted by a Cauchy model (fixed: A=1.46, B=0, C=0, thickness was fitted).

Antifouling and inhibition of cell adhesion

Antifouling tests were performed with PEO-like films prepared by APPD in the PlasmaSpot® with a ring nozzle and in the environment with low air content on SiO_2 substrates with 100 nm thermal oxide. Two scans of deposition were used, with a precursor gas flow of 0.8 slm and a plasma power of 90 W. After film deposition, the samples were soaked for one hour in deionized water and blown dry with nitrogen to

remove any non-crosslinked material. This makes sure that the loss of material during the incubation with fluorescent antibodies and subsequent wash is minimal, as most of the material loss occurs in the first 10 minutes of soaking (Supplementary figure 4). As controls, SiO_2 substrates with 100 nm thermal oxide either non-coated or coated with a 3-[methoxy(polyethyleneoxy)6-9]propyltrimethoxysilane (PEG-SAM) or an azidoundecyltrimethoxysilane (Azide-SAM) . For PEG-SAM deposition, the samples were submerged in a solution containing 0.5 v-% of 3-[methoxy(polyethyleneoxy)6-9]propyltrimethoxysilane, 0.08 v-% acetic acid in toluene for 12 hours, followed by sonication in acetone and isopropanol. For Azide-SAM deposition, the samples were loaded into a home-built stainless-steel vacuum chamber as described in [39]. The deposition time was two hours, using 120 µL of 11-azidoundecyltrimethoxysilane at 145 ˚C at a pressure of 25 mbar.

The antifouling properties were quantified using fluorescence microscopy (Zeiss LSM 780 confocal microscope). The samples were subsequently incubated for 30 minutes with 5 µL droplets of an antibody solution (200 µg/mL Anti-mouse IgG antibody labelled with a Atto647N fluorescent dye in 150 mM phosphate buffered saline (PBS) PH 7.4). After incubation the samples were thoroughly washed with PBS buffer and DIW to remove all salt residues before inspection with the microscope. For cell adhesion testing, neonatal Human Dermal Fibroblasts (nHDF, ATCC PCS-201-010) were grown in a cell culture incubator (37°C, 100% humidity, 5% CO_2) in Dulbecco's modified Eagle's medium/Nutrient mixture F12 with GlutaMAX supplement (Gibco™), containing 10% foetal bovine serum (Gibco™) and 1% Penicillin-Streptomycin (10 000 U/mL, Gibco™). Cells were then detached from the culture flask with 0.05% trypsin-ethylenediaminetetraacetic (Gibco™) and resuspended in culture medium at a concentration of $1.25x10^5$ cells/mL. To prepare antifouling coating samples for cell culture, SiO_2 substrates with thermal oxide comprising either PEG-SAM or 2EGDVE coatings were sterilized with 70% ethanol and blow-dried with nitrogen gas. Then, modified Culture-Inserts 2 Well (IBIDI) were glued on the samples. For the 2EGDVE coated sample, the culture insert overlapped a coated and an uncoated area. Finally, 240 µL of cell suspension (30 000 cells) was deposited in each insert, and the samples were put in the incubator for 24 h.

Before imaging, the medium was removed from the culture inserts and replaced with 300 µL of phenol red-free Hank's Balanced Salt Solution containing Calcium and Magnesium (Gibco™) containing 0.5 µg/mL of viability stain Calcein Red-Orange AM (Invitrogen™) and 1 µg/mL of nuclear stain Hoechst 34580 (BD Biosciences). Cells were incubated with the dyes for 30 minutes before imaging with a Zeiss LSM 780 confocal microscope using standard emission and excitation filter sets.

Results and discussion

Impact of nozzle and air environment during APPD

Different shapes of 3D-printed nozzles are used to shield the reaction area from air (Figure 2a). In this reaction area, the air content is reduced by the flow of the plasma gas and dilution gas. However, small amounts of air can unintentionally reach the reaction area and interact with the plasma and activated precursor molecules. Residual N_2, H_2O and/or O_2 species can potentially influence the plasma chemistry as well as the polymerization process and film formation. We therefore investigate the impact of the nozzle shape and we compare the deposition in a normal air environment (21% O_2 in N_2) with deposition in an environment with low air content (O_2 < 0.2% in Ar).

Impact of nozzle geometry on air contamination by CFD simulation

The concentration of air during deposition in the reaction area and inside the nozzle was simulated using a CFD model for two nozzle shapes: a line and a ring nozzle (Figure 2c). The simulation setup is visualized in Supplementary figure 1. We considered a gap of 3 mm between the nozzle and the substrate surface, 5.8 slm argon through the precursor gas inlet and 80 slm argon through the plasma gas inlet.

The argon flux through the concentric precursor inlet and plasma inlet greatly reduces the mole fraction of air (Figure 3). Detailed heat maps of the air distribution inside the nozzle are included in Supplementary figure 2a-c. The nozzle geometry affects the remaining air content and its spatial distribution in both the nozzle volume itself and the reaction area, i.e. region between the nozzle and substrate. The line nozzle is more effective in reducing the air content inside the nozzle: we observe air levels below ~0.001% inside the line nozzle, as compared to ~0.07% as the upper level inside the ring nozzle (Figure 3a). This difference may be related mainly to the area of the nozzle exit, which is smaller for the line nozzle compared to the ring nozzle. This results in higher gas velocities, which prevents vortices of air entering the nozzle, as can be seen in Supplementary Figure 2e-f.

The nozzle geometry also affects the air content in the reaction area between the nozzle and substrate. The line nozzle again gives a lower air content than the ring nozzle. On the center axis at the substrate, the air levels are 0.04 % for the line nozzle compared to 0.10% for the ring nozzle (Figure 3a). For both nozzles, the air levels strongly increase along the line scan in the horizontal direction scanning from center towards the edge of the nozzle (Figure 3b). The line scan along the long axis of the line nozzle shows that the air levels are smaller than 0.10% in the volume between the nozzle and the substrate, but rapidly increase underneath the nozzle walls (Figure 3b). The horizontal line scan along the short axis of the line nozzle also shows that the low air levels are limited to the very center region, whereas the air levels

strongly increase near the wall of the nozzle (Figure 3b). The ring nozzle allows more air to enter in the volume between the nozzle and the substrate, with the mole fraction of air rapidly increasing from ~0.10% in the center to ~1% underneath the nozzle wall, and increase further after the nozzle wall (Figure 3b).

To conclude, when using the line nozzle the air contamination is concentrated mainly in the volume between the nozzle and the substrate, with estimated N_2 and O_2 concentrations up to 0.0312% and 0.0084%, respectively (assuming 78% N_2 and 21% O_2 in air). As such, the presence of N_2 and O_2 contamination could affect the APPD process and properties of deposited films. On the other hand, when using the ring nozzle the air contamination is substantial in the reaction area (Figure 3) as well as in the nozzle volume close to the plasma discharge region (Supplementary figure 2). The estimated N_2 and O_2 concentrations range up to 0.78% and 0.21% at the plasma discharge electrode. This could have a more substantial impact on the APPD process by affecting the composition of the plasma by the generation of ROS and RNS and/or by quenching of the plasma [34,35]. Finally, we note that the distance between the discharge electrode and substrate is smaller for the ring nozzle (1.8 cm) as compared to the line nozzle (3.3 cm) which also will potentially affect the process.

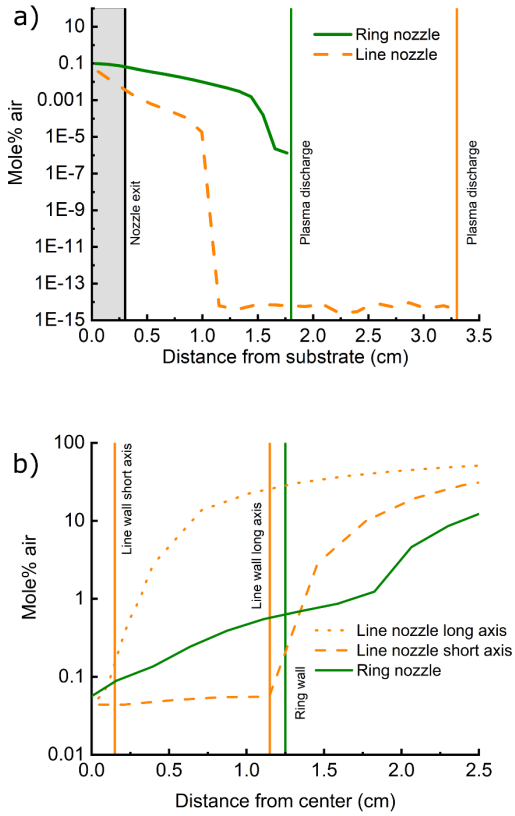

Figure 3: Line scans of the mole% of air a): Along the central axis, starting at, and perpendicular on the substrate, the region between the nozzle and the substrate is indicated in grey, b): starting in the centre along the horizontal axis at the substrate along the long and short cross section of the line nozzle, and radially outwards for the ring nozzle.

Film thickness and stability in deionized water

To study the impact of air contamination on the deposition rate, we investigated deposition with both nozzle types in standard air and environment with low air content by means of growth curves. Figure 4a shows the film thickness, as determined by ellipsometry, as a function of the number of scans for APPD with an atomizer gas flow of 0.8 slm, corresponding to a precursor mass flow of ~7.5 mg/min. The thickness increases linearly with the number of scans for all considered deposition conditions. There is slightly more material deposited during the first scan. Presumably, this can be attributed to heating of the substrate during deposition, which reduces the deposition rate by evaporation of precursor and/or desorption of intermediate species from the substrate. The deposition rates are determined using a linear fit and are reported in Table 1.

The air concentration in the environment affects the growth rate. For both nozzles, deposition in the environment with low air content increases the deposition rate. The impact of reduced air content in the environment is more pronounced for the ring nozzle: the growth rate increases from 55 nm/scan to 118 nm/scan for the ring nozzle and from 43 nm/scan to 57 nm/scan for the line nozzle. This is consistent with the CFD results, where we showed that the line nozzle is better compared to the ring nozzle in shielding the nozzle volume and the reaction area from air. The deposited thickness per scan, between 50 and 100 nm, is high considering that the plasma is expected to mainly have impact at or near the surface. We note that there are multiple passes per scan, considering the scanning pattern and nozzle geometry outlined in Figure 2.

The deposition rates for the line nozzle are lower than for the ring nozzle when we perform depositions in the environment with low air content. This might be explained by the geometry of the nozzle. As the line nozzle is more narrow, part of the precursor can adsorb or impact on the inner surface of the nozzle and result in deposition there, which was visible when inspecting the nozzle after deposition. Another potential explanation is the difference in nozzle geometry, which might change the amount of precursor being carried away into the environment instead of impacting on the substrate. A final potential explanation is the distance between the plasma discharge region and the substrate, which is larger for the line compared to the ring nozzle. This could reduce the amount of active species that reach the substrate.

Next, we investigate if the nozzle type and the presence of air affects the stability of the films in DIW. The film stability is defined as the percentage of the film thickness that remains on the surface after a 10

minutes soak in DIW, as measured with ellipsometry. Films deposited in air with the line nozzle have a stability between 20% and 50%. The stability of the films deposited with the line nozzle increases with the number of scans, which can potentially be explained by post-curing by UV photons, typically emitted by argon dielectric barrier discharges [34], of the already deposited material during the following scan. Films deposited with the ring nozzle are less stable and are completely removed upon soaking (Figure 4b). In contrast, films deposited in an environment with low air content with both nozzles have a better film stability of ~85%. This suggests that the presence of air has an important negative impact on the stability of the deposited films.

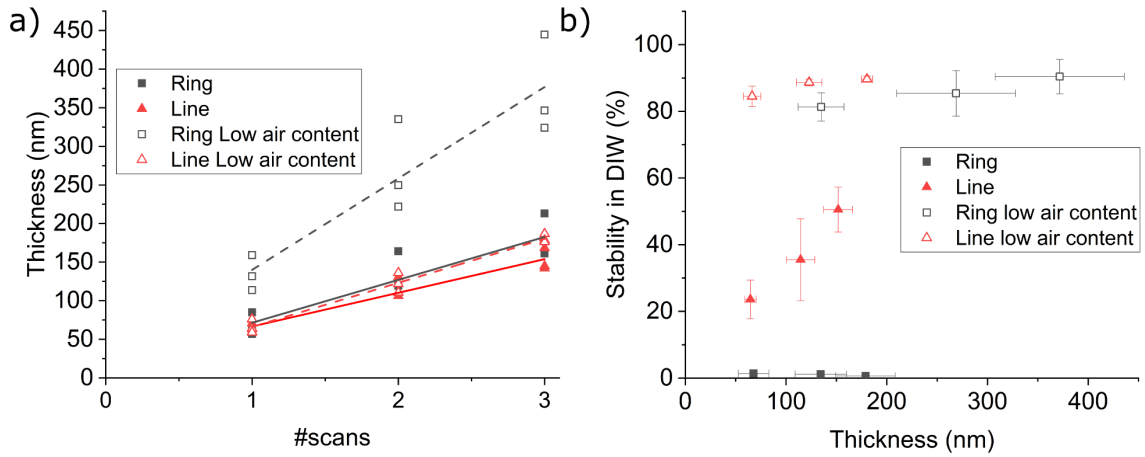

Figure 4: a): thickness in function of the number of scans for 2EGDVE films deposited at 0.8 slm atomizer gas flow. Depositions were performed with both the ring and line nozzle, with and without environment air. Linear fit with dashed lines for the low air content films b): Percentage of the film thickness remaining after a 10 minutes DIW soak, as determined by ellipsometry in function of the original film thickness. Error bars are standard deviation from three separately deposited films.

Table 1: Linear fit of the film thickness in function of the number of scans for 2EGDVE films deposited at 0.8 slm atomizer gas flow. Depositions were performed with both the ring and line nozzle, with and without environment air.

	Line nozzle Std air content	Line nozzle Low air content	Ring nozzle Std air content	Ring nozzle low air content
Intercept	23 ± 10	9 ± 8	16 ± 20	21 ± 43
Slope	43 ± 5	57 ± 4	55 ± 9	118 ± 20
R^2	0.92	0.97	0.83	0.83

Characterization of film composition by FT-IR

To study the impact of the air during deposition on the chemical composition of the films, and to better understand the differences in film stability, we investigate the transmission FT-IR spectra of the deposited films (Figure 5). The spectrum of the 2EGDVE precursor is also shown for comparison. on

Symmetric and asymmetric CH_2 stretching vibrations are visible in the spectra of the precursor and the deposited films. The CH_2 deformation vibration at 1455 cm^{-1} is also observed in the films, suggesting retention of the CH_2-CH_2 units during APPD. A wide band around 1100 cm^{-1} most likely contains the asymmetric CH_2-O-CH_2 stretch of the ether units, which were also observed in the precursor spectrum at 1130 cm^{-1}.

The spectra also show clear signs of reactions between the precursor and the plasma during APPD. The C=C stretch that appears as a doublet band in the precursor spectrum, located at 1636 cm^{-1} and 1618 cm^{-1} (due to blocked rotation around the oxygen atom adjacent to the vinyl group [40]) is greatly reduced in the spectra of the deposited films. In addition, the bands corresponding to =CH rocking vibrations (1320 cm^{-1}) and =CH-O-CH_2 bond stretch (1200 cm^{-1}) of the vinyl ether are not discernible in the spectra of the deposited films. This indicates that most of the vinyl ether end groups have reacted during APPD for all tested conditions, regardless of the film stability. We also observe bands in the spectra of the deposited films that were not observed in the spectrum of the precursor. The wide band around 3500 cm^{-1} can be attributed to OH-stretching of an alcohol and not to water because no peaks related to water scissor vibration at 1640 cm^{-1} are present. We also observe a new band around 1727 cm^{-1} that can be attributed to C=O stretching. Interestingly, the intensity of the C=O band in the spectra of the deposited films strongly depends on the nozzle type and the air content in the environment during deposition. The highest intensity is observed for the least stable films that are deposited with the ring nozzle in the standard air environment.

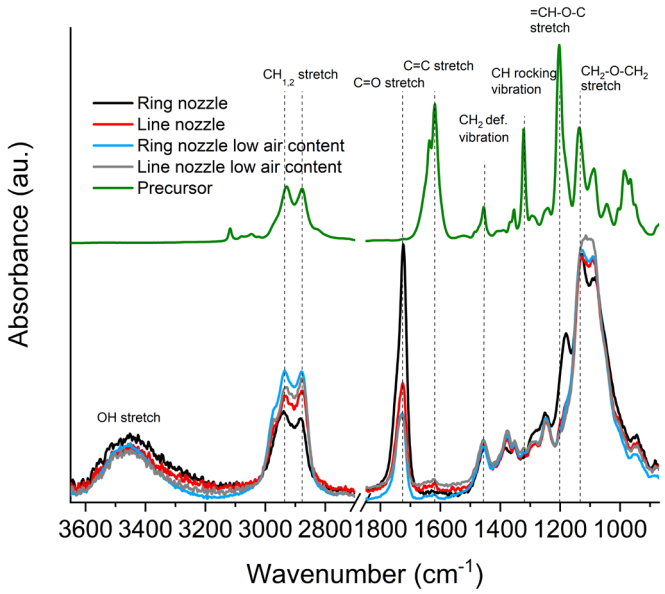

Figure 5: Transmission FT-IR spectra of 2EGDVE films deposited with 2 scans. The film spectra were normalized to the film thickness as obtained by ellipsometry.

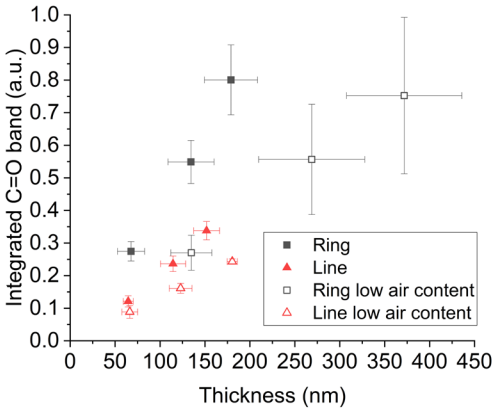

Figure 6: Plot of the integrated C=O band in the transmission FT-IR spectrum, in function of the thickness of the film. Data for 2EGDVE films deposited at 0.8 slm atomizer gas flow. For every condition, 1,2 and 3 scan films are included.

To further investigate the impact of air during APPD on the formation of C=O bonds, we plot the integrated area of the C=O band in the transmission IR spectrum as a function of the film thickness for the various deposition conditions (Figure 6). For similar film thicknesses, deposition with the line nozzle clearly yields films with a lower concentration of C=O bonds compared to the ring nozzle. The lower concentration of C=O bonds in the films could be related to the lower air-content during deposition with the line nozzle, as was suggested by the CFD simulations. The impact of air on the C=O concentration in the films is further

supported by the depositions in the environment with low air content: for deposition with the ring nozzle, the C=O band is strongly reduced when the air content in the environment is reduced. For deposition with the line nozzle this reduction is also observed, but the impact is smaller as the nozzle itself reduces the air in the deposition area. For all conditions, the trends in composition are consistent for various film thicknesses.

Characterization of film composition by XPS

The composition of the top ~10 nm of the deposited films is further analysed by XPS. No silicon or nitrogen are detected in any of the APPD films (Supplementary Figure 5). The absence of peaks related to Si indicates that the substrate is fully covered and that the layers are free of pinholes that reach the substrate. The absence of nitrogen shows that reactive nitrogen species, if present during APPD, are not incorporated in the film. Figure 7 shows the high resolution C 1s spectra. The corresponding atomic percentages of the different C chemical states after deconvolution are reported in Table 2, together with the atomic ratio of oxygen and carbon.

For all deposition conditions, the oxygen/carbon ratio is higher as compared to the precursor stoichiometry of 0.38. This shows that either volatile carbon reaction products are generated, or oxygen is incorporated in the deposited film, which is common for plasma deposition when the films are exposed to air during or after deposition [30,41]. The oxygen/carbon ratio is largest for the film deposited with the ring nozzle in standard air environment (0.71), i.e. the process condition that is expected to be most affected by air contamination. The oxygen/carbon ratio significantly decreases to 0.51 when using the line nozzle in standard air environment. The environment with low air content is also effective in reducing the oxygen/carbon ratio of the films from 0.71 to 0.52 for the ring nozzle.

The chemical bonding of O and C is investigated further by analysing the C 1s spectrum, that shows peaks related to the presence of C-C or C-H bonds, C-O bonds, C=O or O-C-O bonds and O-C=O bonds (figure 7). The decrease in O/C ratio for deposition with the line nozzle compared to the ring nozzle goes together with lower relative C=O and O-C=O components, especially for depositions in standard air environment (9% versus 18% for C=O, 4% versus 12% for O-C=O, for line versus ring nozzle, respectively), in agreement with the FT-IR results. We also observe the lower fraction of C=O and O-C=O components for deposition using the ring nozzle the environment with low air content, in agreement with the FT-IR results. These observations suggests that the presence of air during deposition affects the formation of C=O bonds in the films, consistent with the FT-IR results.

It has been reported that the antifouling properties of PEO-containing films are affected by the content of C-O-C bonds in the films [19]. The high intensity of the C-O band in FT-IR around 1100 cm^{-1} together

with the low intensity of the OH band indicates that the C-O component detected with XPS (Table 2) mainly consists of C-O-C and the contribution of C-OH bonded carbon is small. The films deposited with the line nozzle and in the environment with low air content show more than 64% of C-O bonded carbon (Table 2). This is more than the 60% content of C-O-C bonded carbon often mentioned to achieve good antifouling behaviour in literature [24].

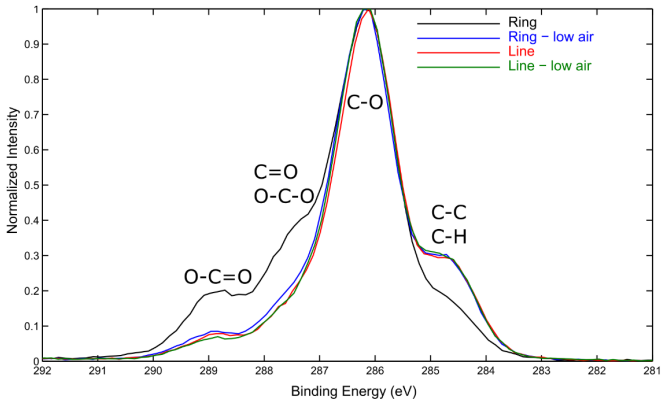

Figure 7: C 1s peak in the high resolution XPS spectrum. XPS was performed on films deposited with 2 scans.

	O/C ratio	CH, C-C at%	C-O-C, C-OH at%	C=O, O-C-O at%	O-C=O at%
Ring nozzle, standard air content	0.71	11	59	18	12
Line nozzle, standard air content	0.51	21	65	9	5
Ring nozzle, low air content	0.52	19	65	11	5
Line nozzle, low air content	0.50	20	66	9	4
Precursor (calculated)	0.38	25	75	0	0
PEG-SAM	/	17	79	5	0

Table 2: XPS results: Second column contains atomic ratio of oxygen and carbon in the films, based on the XPS C 1s and O1s spectra. The other columns represent atomic carbon concentrations of the different chemical states, based on the fitting of the C 1s peak in the high resolution XPS spectrum. From low to high binding energy representing 4 peaks containing mainly C-C and C-H bonds, C-O bonds, C=O or O-C-O bonds and O-C=O bonds. XPS was performed on films deposited with 2 scans.

Impact of air on the film formation

The presence of air can impact the film formation during APPD in two ways. First, O_2 can react with carbon radical sites during radical chain growth polymerization, yielding peroxyl radicals and hydroperoxides with lower reactivity (Figure 8) [29,31,32]. Both functions can then react further to form carbonyl, hydroxyl or ester functions. Second, air can also drastically change the reactive species in a plasma. In contact with plasma, air is known to form reactive oxygen species (ROS) such as HO•, O_2^-, H_2O_2, atomic O, and reactive

nitrogen species (RNS) such as NO_x, NO^+, NO^- [34,35]. These species can further change the plasma chemistry and film composition [42].

Based on the observations with FT-IR and XPS, we propose a similar mechanism for the PEO-like film formation during APPD in an open-air environment (Figure 8). We propose that the vinyl bonds of the 2EGDVE precursor are activated by the plasma, which is in line with the disappearance of the C=C bond stretch (FT-IR), regardless of the air content in the open environment and nozzle type. The formation of C=O, O-C-O and O-C=O groups is observed with both FT-IR and XPS and the oxygen/carbon ratio of the films increases when the air content during APPD increases, suggesting that the uptake of oxygen is related to the presence of air. We propose that the subsequent polymerization process is inhibited in the presence of air, which is suggested by low deposition rates. The poor stability of the films in DIW may be related to termination reactions forming carbonyl and hydroxyl functions.

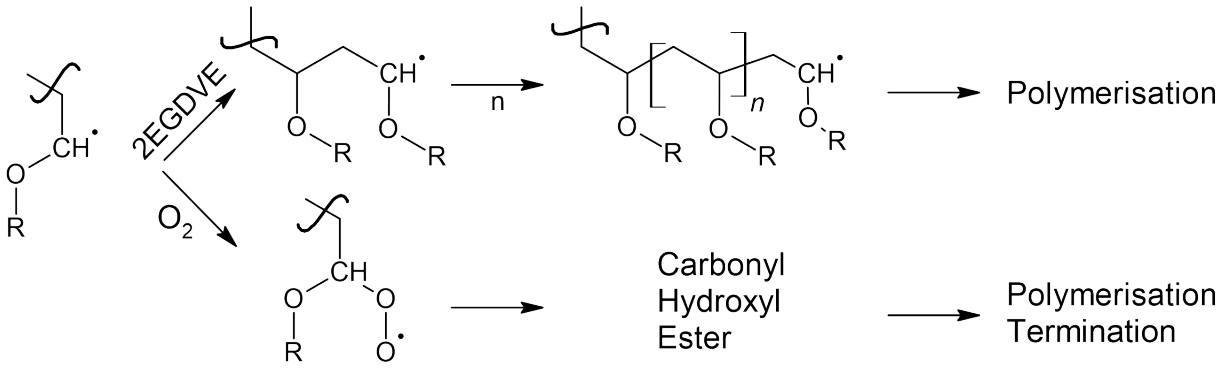

Figure 8: Suggested polymerization and termination mechanism in presence and in absence of oxygen.

Antifouling properties

Finally, we investigated the antifouling properties of APPD PEO-like films in the environment with low air content as such coatings should prevent the non-specific binding of proteins from a solution to the substrate [5]. This was tested by measuring the binding of fluorescently labelled IgG antibodies, which is a relevant test for antifouling coatings, as antifouling coatings are often used to prevent the non-specific binding of antibodies in immunoassays. The antifouling performance of the APPD PEO-like film was compared with three reference samples: a PEG-SAM with high concentration of C-O bonded carbon (low-fouling, Table 2) [43], an SiO_2 with thermal oxide substrate (high fouling) and an azide-SAM (high fouling). Figure 9 shows the remaining fluorescent intensity measured after incubation of the film with the fluorescent antibody solution followed by rinsing. As expected, the SiO_2 with thermal oxide and azide-SAM coated samples show high fluorescent intensities that signal high fouling. The APPD PEO-like film shows fluorescent intensities comparable to the PEG-SAM layer, and strongly reduced fluorescent intensities

compared to the SiO_2 with thermal oxide and azide-SAM sample. The observed antifouling behaviour agrees with the high percentage of C-O bonded carbon in the films, as observed by XPS. We note that the morphology of the films after incubation with antibodies is not characterized. However, the dimensions of an antibody are very small (~2nm X 7 nm) and its attachment to the sensor surface should not have a strong impact on the morphology.

Secondly, the cell adhesion on the film was tested by attempting to grow human fibroblasts on the surface of the films. Fibroblasts secrete an extensive set of extracellular matrix proteins that mediate cell adhesion. These molecules adhere to the surface, making it appropriate for cell adhesion. An antifouling coating, however, should not permit cell adhesion to the surface by preventing the adsorption of fibroblast-secreted proteins. Figure 10a shows a fluorescence microscopy image of a substrate partially coated with 2EGDVE and on which human fibroblasts were grown for 24 h. While the cells in the upper half of the image (uncoated) show the morphology of healthy adherent cells, only few clustered cells are found in the bottom half (coating) and display rounded shapes typical of cells unable to attach to a surface. In Figure 10b, a fluorescence microscopy image of a reference PEG-SAM film incubated with cells is shown. The same behaviour as on the 2EGDVE coated sample is observed, with almost no adherent cells and a few regions with clustered cells, indicating that the coating had the desired effect of preventing cell adhesion and growth. Moreover, those results show that the coating retained good antifouling properties and can withstand cell culture in an aqueous environment up to 24 hours. While long term testing is still required, it may also suggest that no toxic compounds are released in the culture medium, and that the 2EGDVE coating could be used in devices required to be biocompatible.

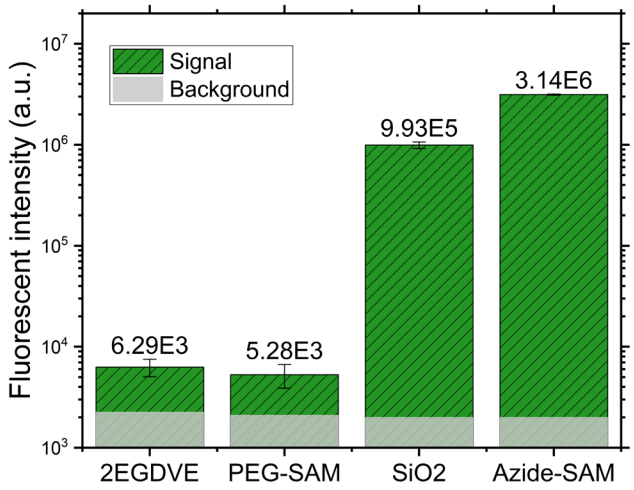

Figure 9: Graph of the fluorescent intensity, plotted on a logarithmic scale, after exposure with fluorescent antibodies for the different films. Error bars based on standard deviation based on three measurements at different locations on the same sample.

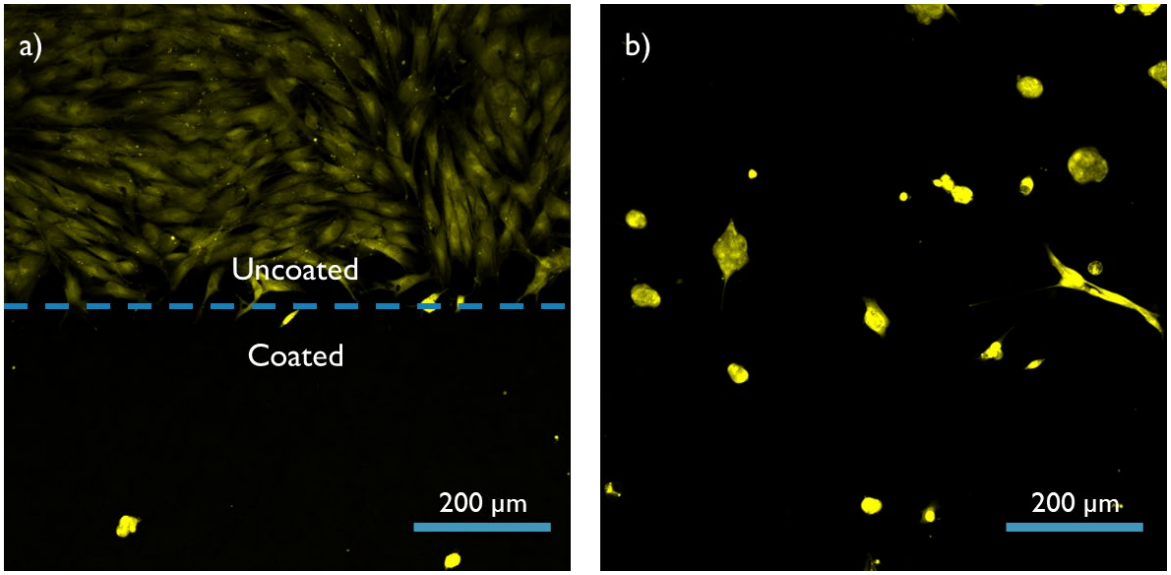

Figure 10: Fluorescence microscopy images of two samples, incubated for cells for 24 hours. a): a sample of which the upper half is untreated, and the lower half is coated with 2EGDVE, b): a substrate fully coated with a PEG-self assembled monolayer.

Conclusions and outlook

While open-air CAPjet APPD processes attract increasing attention due to their versatility and potential for scaling up the production, the impact of the deposition environment is often less understood, with unknown consequences for the composition and properties of the deposited coatings. In this work we investigated the impact of the air environment on the APPD of PEO-like antifouling coatings from a

vinylether precursor. We have investigated the thickness, composition, stability in DIW and the antifouling properties of the obtained coatings. It was found that air affects the APPD process: it leads to introduction of carbonyl groups shown by both FT-IR and XPS, and a reduction of the deposition rate and stability of the deposited films in water. We showed that the nozzle shape can be used to reduce the air content in the reaction area and suppress the formation of carbonyl and carboxyl groups, with the resulting coatings showing improved stability. FT-IR and XPS measurements showed that the ethylene oxide repeats from the precursor were retained, and the resulting coatings resisted both non-specific binding by an antibody solution and completely prevent cell-adhesion of fibroblast cells. This work shows that the impact of air cannot be neglected when using open-air plasmas, and understanding the role of air is important to obtain the reliable and stable coatings and might also be important for other precursor chemistries. Further research is needed to verify the reaction mechanism and to get atomistic insight into the reactions and resulting structure of the deposited films. Characterization of the plasma is needed to further understand the impact of air on the active species in the plasma. Furthermore, characterization of the aerosol size for precursors with different viscosity and vapor pressure would be beneficial to gain more understanding of the deposition process.

Conflicts of interest

Bernard Nisol is an employee of Molecular Plasma Group

Acknowledgements

T. Dekoster is SB PhD fellow at FWO (1SD6623N)

References

[1] A.P.F. Turner, Biosensors: sense and sensibility, Chemical Society Reviews 42 (2013) 3184. https://doi.org/10.1039/c3cs35528d.

[2] C.C. O'Mahony, V. Gubala, R.P. Gandhiraman, S. Daniels, J.S. Yuk, B.D. MacCraith, D.E. Williams, Improving the sensitivity of immunoassays with PEG-COOH-like film prepared by plasma-based technique, Journal of Biomedical Materials Research Part A 100A (2012) 230–235. https://doi.org/10.1002/jbm.a.33268.

[3] A.N. Raditya, D. O'Hare, Review—Electrochemical Sensor Biofouling in Environmental Sensor Networks: Characterisation, Remediation and Lessons from Biomedical Devices, J. Electrochem. Soc. 167 (2020) 127503. https://doi.org/10.1149/1945-7111/aba931.

[4] M. Shen, Y.V. Pan, M.S. Wagner, K.D. Hauch, D.G. Castner, B.D. Ratner, T.A. Horbett, Inhibition of monocyte adhesion and fibrinogen adsorption on glow discharge plasma deposited tetraethylene glycol dimethyl ether, Journal of Biomaterials Science, Polymer Edition 12 (2001) 961–978. https://doi.org/10.1163/156856201753252507.

[5] R. Konradi, C. Acikgoz, M. Textor, Polyoxazolines for Nonfouling Surface Coatings - A Direct Comparison to the Gold Standard PEG, Macromolecular Rapid Communications 33 (2012) 1663–1676. https://doi.org/10.1002/marc.201200422.
[6] S.-W. Lee, P.E. Laibinis, Protein-resistant coatings for glass and metal oxide surfaces derived from oligo(ethylene glycol)-terminated alkyltrichlorosilanes, Biomaterials 19 (1998) 1669–1675. https://doi.org/10.1016/S0142-9612(98)00044-1.
[7] M. Cerruti, S. Fissolo, C. Carraro, C. Ricciardi, A. Majumdar, R. Maboudian, Poly(ethylene glycol) Monolayer Formation and Stability on Gold and Silicon Nitride Substrates, Langmuir 24 (2008) 10646–10653. https://doi.org/10.1021/la801357v.
[8] A. Papra, N. Gadegaard, N.B. Larsen, Characterization of Ultrathin Poly(ethylene glycol) Monolayers on Silicon Substrates, Langmuir 17 (2001) 1457–1460. https://doi.org/10.1021/la000609d.
[9] W. Feng, S. Zhu, K. Ishihara, J.L. Brash, Protein resistant surfaces: Comparison of acrylate graft polymers bearing oligo-ethylene oxide and phosphorylcholine side chains, Biointerphases 1 (2006) 50–60. https://doi.org/10.1116/1.2187495.
[10] C. Rodriguez-Emmenegger, M. Houska, A.B. Alles, E. Brynda, Surfaces Resistant to Fouling from Biological Fluids: Towards Bioactive Surfaces for Real Applications, Macromolecular Bioscience 12 (2012) 1413–1422. https://doi.org/10.1002/mabi.201200171.
[11] S. Tugulu, H.-A. Klok, Stability and Nonfouling Properties of Poly(poly(ethylene glycol) methacrylate) Brushes under Cell Culture Conditions, Biomacromolecules 9 (2008) 906–912. https://doi.org/10.1021/bm701293g.
[12] H. Ma, M. Wells, T.P. Beebe, A. Chilkoti, Surface-Initiated Atom Transfer Radical Polymerization of Oligo(ethylene glycol) Methyl Methacrylate from a Mixed Self-Assembled Monolayer on Gold, Advanced Functional Materials 16 (2006) 640–648. https://doi.org/10.1002/adfm.200500426.
[13] J. Sung, D.G. Lee, S. Lee, J. Park, H.W. Jung, Crosslinking Dynamics and Gelation Characteristics of Photo- and Thermally Polymerized Poly(Ethylene Glycol) Hydrogels, Materials 13 (2020) 3277. https://doi.org/10.3390/ma13153277.
[14] J.W. Hwang, S.M. Noh, B. Kim, H.W. Jung, Gelation and crosslinking characteristics of photopolymerized poly(ethylene glycol) hydrogels, J. Appl. Polym. Sci. 132 (2015). https://doi.org/10.1002/app.41939.
[15] F. Palumbo, P. Favia, M. Vulpio, RF Plasma Deposition of PEO-Like Films: Diagnostics and Process Control, Plasmas and Polymers (2001) 12. https://doi.org/10.1023/A:1013144612953.
[16] M.N. Mar, B.D. Ratner, S.S. Yee, An intrinsically protein-resistant surface plasmon resonance biosensor based upon a RF-plasma-deposited thin film, Sensors and Actuators B: Chemical 54 (1999) 125–131. https://doi.org/10.1016/S0925-4005(98)00330-X.
[17] F. Brétagnol, M. Lejeune, A. Papadopoulou-Bouraoui, M. Hasiwa, H. Rauscher, G. Ceccone, P. Colpo, F. Rossi, Fouling and non-fouling surfaces produced by plasma polymerization of ethylene oxide monomer, Acta Biomaterialia 2 (2006) 165–172. https://doi.org/10.1016/j.actbio.2005.11.002.
[18] A. Michelmore, P. Gross-Kosche, S.A. Al-Bataineh, J.D. Whittle, R.D. Short, On the Effect of Monomer Chemistry on Growth Mechanisms of Nonfouling PEG-like Plasma Polymers, Langmuir 29 (2013) 2595–2601. https://doi.org/10.1021/la304713b.

[19] E.E. Johnston, J.D. Bryers, B.D. Ratner, Plasma Deposition and Surface Characterization of Oligoglyme, Dioxane, and Crown Ether Nonfouling Films, Langmuir 21 (2005) 870–881. https://doi.org/10.1021/la036274s.
[20] G. Da Ponte, E. Sardella, F. Fanelli, R. d'Agostino, R. Gristina, P. Favia, Plasma Deposition of PEO-Like Coatings with Aerosol-Assisted Dielectric Barrier Discharges: Plasma Deposition of PEO-Like Coatings, Plasma Processes and Polymers 9 (2012) 1176–1183. https://doi.org/10.1002/ppap.201100201.
[21] I. Gordeev, A. Choukourov, M. Šimek, V. Prukner, H. Biederman, PEO-like Plasma Polymers Prepared by Atmospheric Pressure Surface Dielectric Barrier Discharge: PEO-like Plasma Polymers Prepared by Atmospheric Pressure SDBD, Plasma Processes and Polymers 9 (2012) 782–791. https://doi.org/10.1002/ppap.201100213.
[22] I. Gordeev, M. Šimek, V. Prukner, A. Artemenko, J. Kousal, D. Nikitin, A. Choukourov, H. Biederman, Deposition of Poly(Ethylene Oxide)-Like Plasma Polymers on Inner Surfaces of Cavities by Means of Atmospheric-Pressure SDBD-Based Jet, Plasma Processes and Polymers 13 (2016) 823–833. https://doi.org/10.1002/ppap.201500214.
[23] G. Da Ponte, E. Sardella, F. Fanelli, A. Van Hoeck, R. d'Agostino, S. Paulussen, P. Favia, Atmospheric pressure plasma deposition of organic films of biomedical interest, Surface and Coatings Technology 205 (2011) S525–S528. https://doi.org/10.1016/j.surfcoat.2011.03.112.
[24] C.P. Stallard, P. Solar, H. Biederman, D.P. Dowling, Deposition of Non-Fouling PEO-Like Coatings Using a Low Temperature Atmospheric Pressure Plasma Jet, Plasma Processes and Polymers 13 (2016) 241–252. https://doi.org/10.1002/ppap.201500034.
[25] S. Bhatt, J. Pulpytel, S. Mori, M. Mirshahi, F. Arefi-Khonsari, Cell Repellent Coatings Developed by an Open Air Atmospheric Pressure Non-Equilibrium Argon Plasma Jet for Biomedical Applications: Cell Repellent Coatings Developed by an Open Air Atmospheric Pressure, Plasma Processes and Polymers 11 (2014) 24–36. https://doi.org/10.1002/ppap.201300076.
[26] B. Nisol, C. Poleunis, P. Bertrand, F. Reniers, Poly(ethylene glycol) Films Deposited by Atmospheric Pressure Plasma Liquid Deposition and Atmospheric Pressure Plasma-Enhanced Chemical Vapour Deposition: Process, Chemical Composition Analysis and Biocompatibility, Plasma Processes and Polymers 7 (2010) 715–725. https://doi.org/10.1002/ppap.201000023.
[27] B. Nisol, G. Oldenhove, N. Preyat, D. Monteyne, M. Moser, D. Perez-Morga, F. Reniers, Atmospheric plasma synthesized PEG coatings: non-fouling biomaterials showing protein and cell repulsion, Surface and Coatings Technology 252 (2014) 126–133. https://doi.org/10.1016/j.surfcoat.2014.04.056.
[28] D. Merche, N. Vandencasteele, F. Reniers, Atmospheric plasmas for thin film deposition: A critical review, Thin Solid Films 520 (2012) 4219–4236. https://doi.org/10.1016/j.tsf.2012.01.026.
[29] M.I. Hasan, J.L. Walsh, Influence of gas flow velocity on the transport of chemical species in an atmospheric pressure air plasma discharge, Appl. Phys. Lett. 110 (2017) 134102. https://doi.org/10.1063/1.4979178.

[30] J. Friedrich, Mechanisms of Plasma Polymerization - Reviewed from a Chemical Point of View, Plasma Processes and Polymers 8 (2011) 783–802. https://doi.org/10.1002/ppap.201100038.
[31] A. Batan, B. Nisol, A. Kakaroglou, I. De Graeve, G. Van Assche, B. Van Mele, H. Terryn, F. Reniers, The Impact of Double Bonds in the APPECVD of Acrylate-Like Precursors: Double Bonds in the APPECVD of Acrylate-Like Precursors, Plasma Processes and Polymers 10 (2013) 857–863. https://doi.org/10.1002/ppap.201300054.
[32] R. Simič, J. Mandal, K. Zhang, N.D. Spencer, Oxygen inhibition of free-radical polymerization is the dominant mechanism behind the “mold effect” on hydrogels, Soft Matter 17 (2021) 6394–6403. https://doi.org/10.1039/D1SM00395J.
[33] K. Studer, C. Decker, E. Beck, R. Schwalm, Overcoming oxygen inhibition in UV-curing of acrylate coatings by carbon dioxide inerting, Part I, Progress in Organic Coatings 48 (2003) 92–100. https://doi.org/10.1016/S0300-9440(03)00120-6.
[34] K. Takeda, K. Ishikawa, H. Tanaka, M. Sekine, M. Hori, Spatial distributions of O, N, NO, OH and vacuum ultraviolet light along gas flow direction in an AC-excited atmospheric pressure Ar plasma jet generated in open air, J. Phys. D: Appl. Phys. 50 (2017) 195202. https://doi.org/10.1088/1361-6463/aa6555.
[35] R. Reuter, K. Rügner, D. Ellerweg, T. de los Arcos, A. von Keudell, J. Benedikt, The Role of Oxygen and Surface Reactions in the Deposition of Silicon Oxide like Films from HMDSO at Atmospheric Pressure: The Role of Oxygen and Surface Reactions in the Deposition of SiO2 -like Films, Plasma Processes Polym. 9 (2012) 1116–1124. https://doi.org/10.1002/ppap.201100146.
[36] M. Meuris, P. Mertens, A. Opdebeeck, H. Schmidt, M. Depas, G. Vereecke, M. Heyns, A. Philipossian, The IMEC clean : A new concept for particle and metal removal on Si surfaces, Solid State Technology 38 (1995) 109–114.
[37] J. Borek-Donten, B. Nisol, M. Filimon, M. Lopes, D. Collard, M. Chassaing, H. -M. Cauchie, R. Heyberger, The industrial process for virucidal plasma coatings on textiles: From idea to upscaling, Plasma Processes & Polymers 19 (2022) 2100249. https://doi.org/10.1002/ppap.202100249.
[38] K. Jans, Het gebruik van poly-(ethyleenglycol) gemodificeerde trichloorsilanen voor de opbouw van proteïneresistente oxide-oppervlakken, PhD thesis, KU Leuven, 2004.
[39] R. Vos, C. Rolin, J. Rip, T. Conard, T. Steylaerts, M.V. Cabanilles, K. Levrie, K. Jans, T. Stakenborg, Chemical Vapor Deposition of Azidoalkylsilane Monolayer Films, Langmuir 34 (2018) 1400–1409. https://doi.org/10.1021/acs.langmuir.7b04011.
[40] G. Socrates, Infrared and Raman Characteristic Group Frequencies: Tables and Charts, 3rd Edition, 3rd ed., John Wiley & Sons Ltd, 2001.
[41] S. Watson, U. Legrand, R. Arrachepied, B. Nisol, P. Girard-Lauriault, J.R. Tavares, M.R. Wertheimer, Organic coatings from acetylene at atmospheric pressure: UV light versus plasma, Plasma Process Polym 18 (2021) 2000211. https://doi.org/10.1002/ppap.202000211.
[42] K. Acharya, S. Bulou, T. Gaulain, P. Choquet, Area selective atmospheric pressure PECVD of organosilicon precursors: Role of vinyl and ethoxy groups on silicon oxycarbide deposition patterns - A case study, Surface and Coatings Technology 451 (2022) 129001. https://doi.org/10.1016/j.surfcoat.2022.129001.

[43] R. De Palma, Surface engineering : immunosensor interfaces, magnetic biosensors and magnetic nanoparticles, PhD thesis, KU Leuven, 2007. https://imec-publications.be/handle/20.500.12860/11969.

List of Figures

Figure 1: Di(ethylene glycol) divinyl ether (2EGDVE) precursor structure 3
Figure 2: a) Schematic of the plasma deposition tool used for the experiments. b) Schematic of the MPG atomizer used for aerosol generation c) Drawing of the 3D-printed nozzles used to shield the reaction area from air. 4
Figure 3: Line scans of the mole% of air a): Along the central axis, starting at, and perpendicular on the substrate, the region between the nozzle and the substrate is indicated in grey, b): starting in the centre along the horizontal axis at the substrate along the long and short cross section of the line nozzle, and radially outwards for the ring nozzle. 9
Figure 4: a): thickness in function of the number of scans for 2EGDVE films deposited at 0.8 slm atomizer gas flow. Depositions were performed with both the ring and line nozzle, with and without environment air b): Percentage of the film thickness remaining after a 10 minutes DIW soak, as determined by ellipsometry in function of the original film thickness. Error bars are standard deviation from three separately deposited films. 11
Figure 5: Transmission FT-IR spectra of 2EGDVE films deposited with 2 scans. The film spectra were normalized to the film thickness as obtained by ellipsometry. 12
Figure 6: Plot of the integrated C=O band in the transmission FT-IR spectrum, in function of the thickness of the film. Data for 2EGDVE films deposited at 0.8 slm atomizer gas flow. For every condition, 1,2 and 3 pass films are included. 13
Figure 7: C 1s peak in the high resolution XPS spectrum. XPS was performed on films deposited with 2 scans. 14
Figure 8: Suggested polymerization and termination mechanism in presence and in absence of oxygen. 16
Figure 9: Graph of the fluorescent intensity, plotted on a logarithmic scale, after exposure with fluorescent antibodies for the different films. Error bars based on standard deviation based on three measurements at different locations on the same sample. 17
Figure 10: Fluorescence microscopy images of two samples, incubated for cells for 24 hours. a): a sample of which the upper half is untreated, and the lower half is coated with 2EGDVE, b): a substrate fully coated with a PEG-self assembled monolayer 17